Article

The Association between Meteorological Drought and the State of the Groundwater Level in Bursa, Turkey

Babak Vaheddoost [1] , Babak Mohammadi [2,*] and Mir Jafar Sadegh Safari [3]

1   Department of Civil Engineering, Bursa Technical University, Bursa 16310, Turkey;
     babak.vaheddoost@btu.edu.tr
2   Department of Physical Geography and Ecosystem Science, Lund University, Sölvegatan 12,
     223 62 Lund, Sweden
3   Department of Civil Engineering, Yasar University, Izmir 35100, Turkey; jafar.safari@yasar.edu.tr
*   Correspondence: babak.mohammadi@nateko.lu.se

Abstract: This study addressed the intricate interplay between meteorological droughts and groundwater level fluctuations in the vicinity of Mount Uludag in Bursa, Turkey. To achieve this, an exhaustive analysis encompassing monthly precipitation records and groundwater level data sourced from three meteorological stations and eight groundwater observation points spanning the period from 2007 to 2018 was performed. Subsequently, this study employed the Standard Precipitation Index (SPI) and Standard Groundwater Level (SGL) metrics, meticulously calculating the temporal extents of drought events for each respective time series. Following this, a judicious application of both the Thiessen and Support Vector Machine (SVM) methodologies was undertaken to ascertain the optimal groundwater observation wells and their corresponding SGL durations, aligning them with SPI durations tied to the selected meteorological stations. The SVM technique, in particular, excelled in the identification of the most pertinent observation wells. Additionally, the Elman Neural Network (ENN) and its optimized version through the Firefly Algorithm (ENN-FA), demonstrated their prowess in accurately predicting SPI durations based on SGL durations. The results were favorable, as evidenced by the commendable performance metrics of the Normalized Root Mean Square Error (NRMSE), the Nash–Sutcliffe Efficiency (NSE), the product of the coefficient of determination and the slope of the regression line (bR^2), and the Kling–Gupta Efficiency (KGE). Consequently, the favorable simulation results were construed as evidence supporting the presence of a discernible association between SGL and the duration of the SPI. As we substantiate the concordance between the temporal extent of meteorological droughts and the perturbations in groundwater levels, this unmistakably underscores the fact that the historical fluctuations in groundwater levels within the region were predominantly attributable to climatic influences, rather than being instigated by anthropogenic activities. Nevertheless, it is imperative to underscore that this revelation should not be misconstrued as an endorsement of future heedless exploitation of groundwater resources.

Keywords: drought duration; Elman neural network; firefly algorithm; groundwater level; support vector machine

1. Introduction

Extreme weather events are well-known threats around the globe [1]. In particular, drought represents a multifaceted and intricate phenomenon, predominantly contingent upon the temporal and spatial availability of water resources [2,3]. It has the potential to strain agro-food and socio-economic stability to the point of collapse [4,5]. Its genesis lies in the diminishing or outright absence of precipitation, constituting meteorological drought, which subsequently evolves into more intricate hydro-environmental manifestations [6]. These include the depletion of soil moisture, culminating in agricultural drought, as well as the reduction in streamflow rates, representing hydrological drought. Moreover, the dearth of accessible water resources for essential human activities constitutes socio-economic

drought [7]. Throughout history, the climate has undergone significant transformations, primarily driven by natural forces. However, the contemporary climate crisis is inexorably linked to rapid industrialization and the pervasive emission of greenhouse gases. This climate metamorphosis engenders fluctuations in water resource availability, instigating extreme climatic events such as droughts and floods. Nonetheless, the classification of drought hinges on the nature of the available water resources within a specific locale, dictating the norms of climatic conditions in terms of both temporal and spatial dimensions and what can be accepted as a drought for a specific region.

Groundwater, a vital component of the Earth's freshwater resources, constitutes approximately 30 percent of the available freshwater worldwide [8]. In regions where surface water resources are either scarce or unreliable, groundwater emerges as the optimal alternative to meet various water demands. The controlled release of aquifer-stored water through natural or engineered means, including wells, drainage systems, aqueducts, springs, and pumping, underscores the importance of groundwater as a resource. Paradoxically, the abundant availability of groundwater in aquifers can also be a catalyst for droughts, often intertwined with meteorological factors such as precipitation and snow cover, hydrological variables like streamflow, and human-induced activities. It is worth noting that groundwater levels are intricately linked to the recharge processes facilitated by the infiltration of precipitation and snowmelt, particularly in high-altitude areas [9]. Consequently, the nexus between meteorological drought and groundwater drought (excluding fossil or deep reservoirs), exemplified by fluctuations in groundwater levels, plays a pivotal role in shaping local groundwater conditions within a given region [10]. A profound comprehension of the intricate interactions between meteorological phenomena and groundwater dynamics (aquifers) is of paramount significance, particularly in regions characterized by hydrological variability [11–13]. For instance, a comprehensive investigation conducted by Bloomfield and Marchant [14] addressed the relationship between the Standard Precipitation Index (SPI) and the Groundwater Level Index, using a dataset spanning 103 years. Their findings underscored the dependence of Groundwater Level Index autocorrelation on the dominating aquifer flow and storage characteristics. Similarly, Liu et al. [15] conducted a study on the state of groundwater drought and its response to meteorological drought in China. By employing the standardized groundwater level index in conjunction with SPI, they conducted a cross-correlation analysis and identified trends in the respective indices. Their conclusion revealed that the duration and magnitude of groundwater droughts were notably protracted and substantial.

In recent years, substantial strides have been made in predictive modeling techniques harnessing the capabilities of machine learning methodologies [16,17]. In particular, the Elman Neural Network (ENN), enhanced through nature-inspired optimization algorithms, has garnered considerable attention due to its adeptness in deciphering intricate relationships within input and output datasets [18,19]. The ENN, a recurrent neural network architecture, excels in modeling sequential data by accounting for temporal dependencies. Augmenting its capabilities, the Firefly Algorithm (FA) offers an optimization approach inspired by natural phenomena, resulting in refined model architectures and heightened predictive accuracy [20,21]. Similarly, the Support Vector Machine (SVM), a versatile machine learning algorithm, is renowned for its prowess in feature selection and classification tasks [22,23]. Within the context of our study, SVM adeptly identifies the most influential meteorological stations, streamlining our analysis and yielding invaluable insights.

The interplay between groundwater abundance and its correlation with meteorological phenomena in the Bursa region of Turkey presents a distinct case that has not received the depth of investigation it warrants. While prior research has delved into aspects such as thermal waters and local aquifer modeling [24–26], comprehensive analysis of this relationship remains underexplored. Existing studies have primarily focused on the biological and chemical attributes of water content in the region, leaving a gap in our understanding of the intricate dynamics governing the connection between meteorological drought and groundwater level fluctuations. In general, the records pertaining to regional

aquifer groundwater and the hydrogeology of the area have not undergone sufficient investigation. Historically, groundwater has not been the primary water source in this region. However, in light of recent droughts, there is significant potential for groundwater to assume a leading role as the primary water source. However, the traditional approaches toward probing the association between meteorological drought and groundwater level changes have predominantly relied on rudimentary correlations, overlooking the nuanced temporal and spatial intricacies that underlie these associations.

In response to this knowledge gap, we present an exhaustive study employing advanced methodologies to unravel the intricate connections between the SPI and the so-called Standard Groundwater Level (SGL) durations within the vicinity of Mount Uludag. This research also endeavors to elucidate the link between disturbances in the local groundwater table and precipitation deficits within the broader Bursa district. This is primarily imperative in comprehending and strategizing for the potential utilization of subterranean aquifers as a dynamic water resource and fortification against climate perturbations within the locale. To achieve this, we apply the following steps.

(i)   The SGL and SPI for groundwater level and precipitation records are determined.
(ii) The duration curves of SGL and SPI are scrutinized to ascertain the relevance of their respective durations.
(iii) The SVM and Thiessen methods are used alternately in the selection of the most relevant stations.
(iv) The presence of an association between SGL and SPI in the selected stations previously determined either by means of SVM or the Thiessen was tested using cross-correlation analysis and the estimation of SPI durations with the help of SGL durations using ENN empowered by FA.

As a result, by confirming the presence of an association between groundwater disturbances and meteorological droughts, this study is expected to provide grounds for future studies and avoiding encroachments on groundwater sources.

2. Material and Methods

2.1. Study Area

The study area is situated in the northwestern region of Turkey and boasts a notably extensive coastline along the Marmara Sea. Geographically, it spans between the latitudes of $39°34'$ and $40°38'$ N and the longitudes of $28°05'$ and $29°60'$ E, while its topographical variation ranges from sea level up to an elevation of 2543 m above sea level (mASL) at the summit of Mount Uludag. In accordance with the Koppen–Geiger classification system, as elucidated by Kottek et al. [27], the climate within this region falls into two distinct categories: either a warm temperate climate characterized by dry summers and cold-arid temperatures (Csa), or a warm temperate climate marked by dry summers and warm summer temperatures (Csb). The primary river systems coursing through this region include the Mustafakemalpasa, Nilufer, Goksu, Kocadere, Karadere, and Aksudere, all of which play a pivotal role in shaping the riverine hydrology and water cycle within the area. For a comprehensive overview, Figure 1 illustrates the study area, climate regions based on the Koppen–Geiger classification map (attainable in: https://koeppen-geiger.vu-wien.ac.at/present.htm (accessed on 29 October 2023)), and the locations of the selected meteorological stations and observation wells. It also showcases the Thiessen polygons utilized in the meticulous selection process of the optimal meteorological station, a matter we will delve into later.
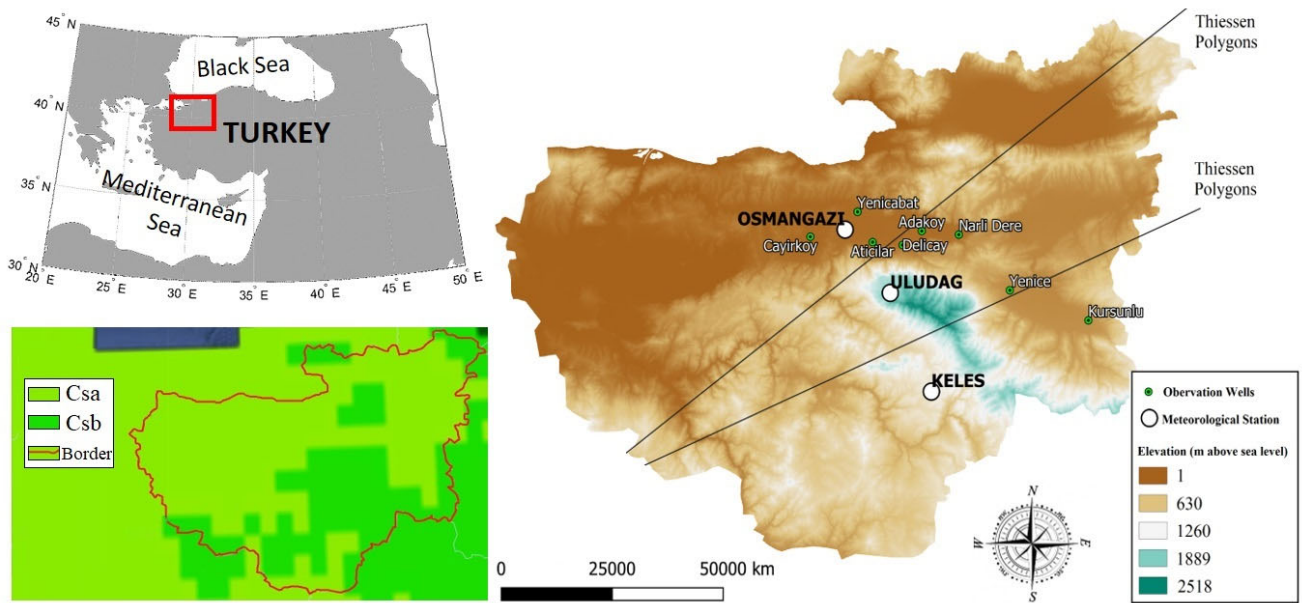
Figure 1. Global positioning of the study area (up left), climate classification [25] (down left), and the selected stations together with the Thiessen polygons (right) used in the analysis.

Notably, all of the meteorological stations are strategically positioned within the lofty Uludag mountain range at high altitudes, while the selected observation wells are situated on hillsides at considerably lower elevations. This positioning was implemented to naturally establish a hydraulic gradient from the meteorological stations towards the groundwater wells on the hillsides. Bearing this key fact in mind, our analysis endeavored to examine the degree of association between precipitation and groundwater time series by investigating both the simultaneous and lagged behaviors of these two crucial variables. Consequently, the analysis employed the monthly time series of precipitation data gathered from three meteorological sites (Osmangazi, Uludag, and Keles) in conjunction with the groundwater level time series data recorded at eight observation wells (Adakoy, Aticilar, Cayirkoy, Delicay, Kursunlu, Narlidere, Yeniceabat, and Yenice) throughout the water year, spanning from 2007 to 2018. For further details regarding the precise locations of the meteorological stations and wells, as well as the fundamental statistical properties of the monthly time series utilized in this analysis, refer to Table 1.

Table 1. Properties of the stations and associated data.

Variable	Station	UTM-X	UTM-Y	Zone	Unit	Mean	Std. Dev.	Min.	Max.
	Keles	69070	442070	35	mm	60.98	48.64	0.00	254.30
Precipitation	Osmangazi	67128	445531	35	mm	59.97	47.98	0.00	396.80
	Uludag	68145	4441805	35	mm	119.64	101.30	0.00	999.50
	Adakoy	688552	4455040	35	mASL	93.38	1.78	89.75	100.00
	Aticilar	677475	4452637	35	mASL	107.14	1.82	103.20	115.54
	Cayirkoy	663459	4453806	35	mASL	160.77	1.19	158.10	165.00
Groundwater Level	Delicay	684217	4452013	35	mASL	123.79	6.59	112.10	147.00
	Kursunlu	726077	4435927	35	mASL	309.31	2.88	305.30	320.00
	Narlidere	696891	4454258	35	mASL	139.53	3.71	132.80	155.00
	Yeniceabat	674075	4459125	35	mASL	71.07	7.20	54.15	87.00
	Yenice	708367	4442375	35	mASL	309.38	2.09	305.27	320.00

Std. Dev.: Standard Deviation; Min.: Minimum; Max.: Maximum.

As depicted in Figure 1 and through the meticulous application of Thiessen polygons, we were able to establish associations between the data records obtained from Uludag, Os-

mangazi, and Keles meteorological stations and from specific locations, at Adakoy, Delicay, Narli Dere, and Yenice; Aticilar, Cayirkoy, and Yeniceabat; and Kursunlu, respectively. This crucial criterion subsequently served as a pivotal determinant in selecting the most suitable input stations for the development of the models, a subject that will be expounded upon in detail later in this analysis.

Table 1 also provides a comprehensive breakdown of the monthly averaged precipitation time series, coupled with the mean groundwater level time series derived from observation wells (from unconfined aquifers) dispersed across our study region. Notably, the station registering the highest mean precipitation rate was Uludag, while the lowest values were associated with the Osmangazi station. Intriguingly, despite Osmangazi's lower average, it recorded maximum precipitation levels surpassing those observed at the Keles station. Turning our attention to the groundwater data, the highest mean groundwater level elevations were documented at the Kursunlu and Yenice stations, while the lowest elevation was recorded at Yeniceabat.

In light of this information, the time series data spanning from January 2007 to November 2018, encompassing a total of 143 months, served as a foundational framework for evaluating the temporal congruence between groundwater and precipitation records.

2.2. Methods

The primary objective of this study was to ascertain the relationship between precipitation patterns at higher elevations and the fluctuations in groundwater levels along hillside regions. This investigation centered on the concurrent dynamics of meteorological drought and perturbations in groundwater levels. The methodology outlined in Figure 2 served as the cornerstone of this research endeavor.
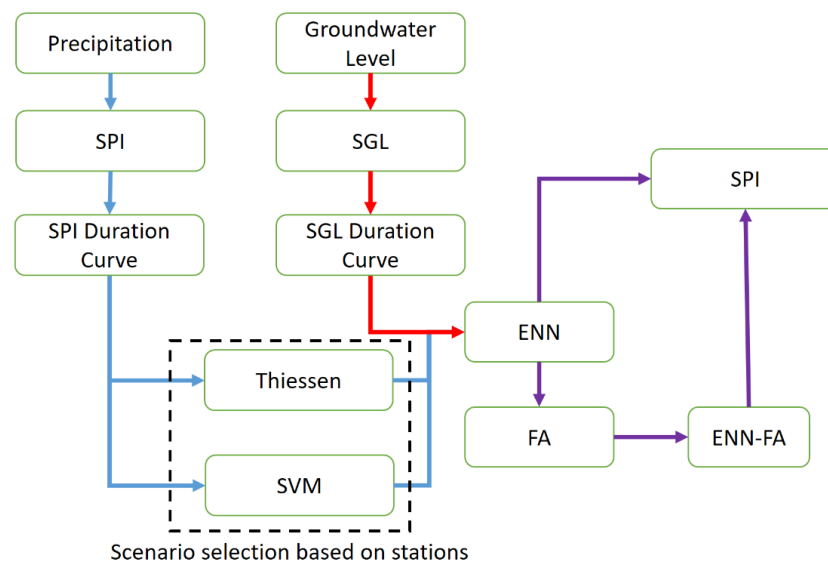
Figure 2. Flowchart of the methods used in the analysis.

In the initial phase, we computed two pivotal indices, the SPI and the SGL. Subsequently, we arranged the time series data for SGL and SPI in ascending order to construct duration curves, thereby determining the corresponding percentiles for both SGL and SPI. Employing a reverse analogical approach, we assessed whether the duration of the SGL index correlates with that of the meteorological drought (i.e., SPI), aiming to confirm or refute any link between groundwater table disturbances and meteorological droughts. To minimize the influence of potential confounding factors, such as neighboring aquifers and surface water, which may impact groundwater conditions on the hillside, we employed SGL as an input parameter and SPI as the output in our simulations.

The identification of the most representative observation wells alternated between employing Thiessen polygons (as depicted in Figure 1) and the SVM as input variables for

our simulation models. Subsequently, the scenarios derived from either Thiessen polygons or SVM served as the basis for forecasting monthly SPI values at meteorological sites. Initially, SPI and SGL functioned as the output and input variables, respectively, within our models. The selection of training and testing data was carried out through a randomized process, aligning with the concurrent duration of SPI and SGL. The ENN was subsequently employed, with the results fine-tuned using the FA, ultimately leading to the introduction of the ENN-FA approach. This approach, along with Thiessen (referred to as Thiessen-ENN-FA) and SVM (known as SVM-ENN-FA) methodologies, will be elaborated upon in greater detail later in this study.

2.2.1. Standard Precipitation Index (SPI)

The Standard Precipitation Index (SPI), a renowned drought index, establishes the water abundance within a particular location by scrutinizing the precipitation deficit or surplus. This index is formulated based on the probability of outcomes derived from pre-fitted probability distributions such as Gamma, Gumbel, among others [28]. These distributions are subsequently employed for standardization, facilitating the quantification of water deficit and surplus intensities.

Within the context of this study, we focused on monthly SPI rates, also referred to as SPI-1 values, in our analysis. However, it is worth noting that the incorporation of long-term deficit/surplus responses can also be achieved using the moving average operator. The preference for SPI-1 over long-term SPI values in this study is attributed to two key factors: the limited availability of data records pertaining to groundwater levels and the inherent complexity associated with short-term drought prediction, which took precedence.

Given the well-established nature of the methodology and equations pertaining to SPI determination, we abstain from reiterating the same details in this section. Interested readers seeking a comprehensive understanding of SPI calculation may refer to the studies conducted by McKee et al. [28], Aksoy [29], and Vaheddoost and Safari [30] for in-depth insights and further applications of the SPI.

2.2.2. Standard Groundwater Level (SGL)

Diverging from prior approaches presented in earlier studies such as those by Bloomfield and Marchant [14] and Liu et al. [15], which introduced the groundwater drought index by employing probability distributions like SPI, this study proposes a simpler standardization method similar to the Z-Score Index (ZSI) for the determination of SGL, as elucidated in Vaheddoost and Safari [30]. The ZSI primarily centers on identifying authentic anomalies within the dataset.

In this context, classical standardization, using the formula $z = \frac{(x - \mu)}{\sigma}$, was implemented and served either as a drought indicator or as a means to highlight anomalies in the temporal correspondence of data. In this equation, the normalized values (z) are derived by subtracting the long-term mean groundwater level (μ) from the monthly groundwater level records (x), thus revealing groundwater level anomalies. These anomalies are then divided by the sample standard deviation of the groundwater level time series (σ).

The acquired SGL time series was subsequently employed in conjunction with the SPI time series in a multitude of analyses aimed at probing the depth of the relationship between SPI and SGL.

2.2.3. Association between SPI and SGL

The monthly time series, coupled with the corresponding duration curves for both SGL and SPI, were instrumental in pursuing this objective. It is postulated that the temporal and spatial congruence of disruptions in the SGL and SPI time series can be regarded as indicative of the propensity for an association between SGL and SPI events. In essence, this implies that if the duration of SPI can be elucidated through SGL duration, and the selection of the study period is conducted on a randomized basis, one can infer that meteorological factors constitute the primary drivers behind groundwater disturbances at the chosen sites.

Hence, in order to validate this hypothesis concerning the relationship between SGL and SPI, the durations of randomly selected SPI events were predicted using the same ranking criteria associated with the corresponding SGL events. As delineated earlier, the Thiessen and SVM methods came into play in the determination of the most optimal scenario-stations and the identification of the most suitable inputs for the models.

2.3. Models

2.3.1. Selection of the Best Meteorological Stations via SVM

The SVM stands as a formidable machine learning algorithm renowned for its effectiveness across a spectrum of tasks, encompassing classification, regression, and feature selection, as evidenced by Gunn [31]. In our study, SVM assumes the role of a feature selection algorithm, its purpose being the identification of the most pertinent meteorological stations for dissecting the interrelation between SPI and SGL durations. This approach enables a meticulous focus on the meteorological stations wielding the greatest influence over predictive accuracy. At the heart of SVM lies the pivotal concept of locating a hyperplane that optimally segregates data points belonging to distinct classes, a notion substantiated by the works of Sugumaran et al. [32] and Cervantes et al. [33]. In the realm of feature selection, SVM undertakes the task of pinpointing the subset of features—in this instance, meteorological stations—that maximizes the demarcation between classes. Within our study, these classes align with SPI and SGL durations.

The SVM process encompasses several crucial phases: (i) Data preparation: each meteorological station's SPI and SGL durations are represented as feature vectors, serving as the foundation for constructing a training dataset for SVM. (ii) Kernel functions: SVM leverages kernel functions to map input data into a higher-dimensional space. This mapping enhances data separability, simplifying the quest for a hyperplane that efficiently distinguishes classes. In our investigation, we explored six distinct kernel functions, including dot, radial, polynomial, neural, ANOVA (analysis of variance), and Epachnenikov [34,35]. (iii) Margin maximization: SVM's primary aim is the discovery of a hyperplane that maximizes the margin, defined as the distance between the hyperplane and the nearest data points from each class. This strategy fosters superior generalization to unseen data. (iv) Support vectors: the data points situated closest to the hyperplane assume the designation of support vectors, playing a pivotal role in determining the hyperplane's position and, consequently, the decision boundaries. (v) Soft margin and regularization: SVM accommodates scenarios where data lacks linear separability by introducing a soft margin, permitting a degree of misclassification. A regularization parameter governs the equilibrium between margin maximization and misclassification minimization.

In our case, SVM undertook the task of ranking the significance of meteorological stations in forecasting SPI and SGL durations. The various kernel functions were systematically applied to the training dataset, resulting in feature rankings that facilitated the selection of the most influential stations. Through the selection of meteorological stations bearing the highest rankings, we aspired to elevate the precision of our predictive model and unearth insights into the primary drivers underpinning the connection between meteorological drought and groundwater level fluctuations.

2.3.2. Application of Elman Neural Network (ENN) Coupled by Firefly Algorithm (FA)

The ENN represents a recurrent neural network architecture with a track record of applications in modeling soil, water, and meteorological time series, as demonstrated in the works of Zhang et al. [36] and Li et al. [37]. ENN's distinct advantage lies in its capacity to capture temporal dependencies within data, rendering it particularly adept for tasks involving sequential patterns and relationships, as underscored by Lu et al. [38]. In this study, we harnessed the ENN as a predictive tool to establish the nexus between SPI and SGL durations, thereby delving into the correlation between meteorological drought and fluctuations in groundwater levels.

The ENN is structured around interconnected layers of processing units, commonly known as neurons, as expounded upon by Li et al. [39]. These neurons are organized into input, hidden, and output layers. Notably, the ENN incorporates a context layer, introducing a feedback loop that allows the network to retain information from previous time steps [40,41]. This contextual information plays a pivotal role in modeling temporal relationships within the data. The ENN comprises four core layers: the input layer, hidden layer, undertake layer, and output layer [42]. The input layer receives SGL data, which are utilized to predict SPI durations. The hidden layer, distinguished by its recurrent connections, captures temporal dependencies and patterns within the data, enabling the ENN to adeptly model sequential information. The undertake layer acts as a memory for the hidden layer output. Ultimately, the output layer generates predictions for SPI durations, predicated upon the acquired knowledge of relationships between input variables. The ENN's recurrent connections enable it to factor in the influence of past observations, rendering it well-suited for capturing dynamic associations between meteorological and groundwater events.

Further refinement of this architecture was achieved through the FA optimization process, enhancing the accuracy of SPI predictions and determining the most suitable network architecture and weightings for the ENN. The FA draws inspiration from nature, specifically the flashing behavior of fireflies, a concept initially proposed by Yang and He [43]. It simulates the movement of fireflies in their quest for optimal solutions within a multidimensional parameter space. In this study, the parameters subjected to optimization encompassed the network architecture (e.g., the number of hidden layers and neurons per layer) and the weights associated with network connections. This tuning process unfolds in several key steps: (i) Initialization: the FA begins by initializing a population of fireflies, where each firefly corresponds to a potential solution, defined by a set of network parameters. (ii) Brightness calculation: each firefly's brightness is determined based on its fitness value, reflecting how well its associated ENN configuration performs in predicting the association between SPI and SGL durations. (iii) Firefly movement: fireflies gravitate towards brighter ones within the search space, guided by a mathematical expression that considers their relative positions and brightness values. This movement aims to converge towards optimal configurations. (iv) Parameter updating: as fireflies move, their parameters are updated to mirror their new positions. These updates translate into adjustments to the ENN's architecture and weights. (v) Iterative process: the movement and parameter updating steps iterate through multiple cycles, enabling fireflies to refine their positions and approach superior solutions. (vi) Convergence: the FA continues to refine firefly positions until a predefined stopping criterion is met, signaling the convergence of the optimization process.

By harnessing the ENN tuned via the Firefly Algorithm, our objective was to discern the optimal network architecture and weightings that facilitate precise predictions of SPI durations predicated on associated SGL durations. For an in-depth exploration of the approach involving the tuning of ANN models via FA, we recommend consulting the work by Mohammadi [21].

2.3.3. Performance Indicators

In order to comprehensively assess the accuracy and reliability of our predictive models, we employed a battery of four distinct performance indicators: the Normalized Root Mean Square Error (NRMSE), the Nash–Sutcliffe Efficiency (NSE), the coefficient of determination multiplied by the slope of the regression line (bR^2), and the Kling–Gupta Efficiency (KGE) [44]. These metrics collectively offer insights into various facets of model performance, encompassing aspects such as error magnitude, precision, linearity, and the overarching concordance between simulated and observed values. In essence, these performance indicators collaboratively furnish a comprehensive evaluation of the models' predictive aptitude, the extent of modeling error, and the overall consistency between the predicted and observed durations of SPI and SGL.

3. Results and Discussion

As elucidated previously, the initial assessment of the selected stations' SGL and SPI values hinged upon the careful examination of time series plots and the geographical congruence between meteorological stations and observation wells. As depicted in Figure 3, the spatial dimension, defined by Thiessen polygons (as previously illustrated in Figure 1), and the temporal dimension, characterized by the resemblance between time series, do not readily reveal a pronounced similarity between monthly SGL and SPI data. However, the broader-scale association between these selected time series does underscore the pertinent connection between precipitation and groundwater abundance. In accordance with the findings of Han et al. [45], who probed the effect of meteorological drought propagation on groundwater level perturbations, it may take several months to discern the groundwater level disturbances linked to an ongoing meteorological drought. Nevertheless, the augmentation of soil moisture expedites the response of groundwater to precipitation during surplus periods due to the stored-full runoff mechanism. Conversely, intensified evapotranspiration and heightened heat wave rates amplify drought propagation during deficit periods. In a recent study by Gong et al. [46], they explored the effects of lag, pooling, lengthening, and attenuation in monitoring the propagation of meteorological drought on groundwater table abundance. Their conclusions highlighted that the impact of lag time in discerning the connection between meteorological and groundwater drought is influenced by factors such as aquifer depth, soil permeability, anthropogenic activities, temporal land use shifts, and prevailing climate conditions.

Therefore, bearing in mind the inherent challenges of scrutinizing short-term periods (i.e., monthly data) in establishing the link between SGL and SPI, the insights gleaned from Figure 3 do provide partial indications of the correlation between precipitation and groundwater levels in the region. Furthermore, considering the local geomorphology, the hydraulic gradient between high-altitude regions and hillsides serves as a compelling rationale for the existence of a relationship between these two variables, namely groundwater and precipitation. This intriguing proposition is subject to further exploration in the ensuing cross-correlation diagram presented in Figure 4.

In the majority of cases, as illustrated in Figure 4, the lagging and leading effects appear to be inconsequential, with the linear correlation scarcely surpassing a meager 0.3. This trend is particularly evident for stations like Delicay, Cayirkoy, and Kursunlu; however, these stations exhibit a somewhat stronger association. Consequently, the limited linear correlation between SPI and SGL time series fails to furnish compelling evidence for a robust linear relationship between precipitation and groundwater levels.

As previously delineated, to enrich our analysis and substantiate the connection between groundwater abundance and meteorological occurrences, we delve into the comparison and prediction of SPI event durations in tandem with SGL durations. Given that neither groundwater nor surface water are likely to exert a significant influence on meteorological precipitation, the prediction of SPI based on SGL offers an alternative perspective on ongoing events within the region. In pursuit of this, we initially derive duration curves for both SGL and SPI, as illustrated in Figure 5. The results reveal a noteworthy resemblance and symmetry between the durations of SGL and SPI. Nonetheless, SPI exhibits some outliers, primarily for the most frequent and extreme events. Evidently, unexpected occurrences, such as extreme or short-term precipitation events, exhibit a weaker association with disturbances in groundwater levels. However, when we consider the broader context, it becomes evident that a substantial correlation and association prevail between hydro-meteorological events, which may occasionally be perturbed by anthropogenic or climate-induced factors.
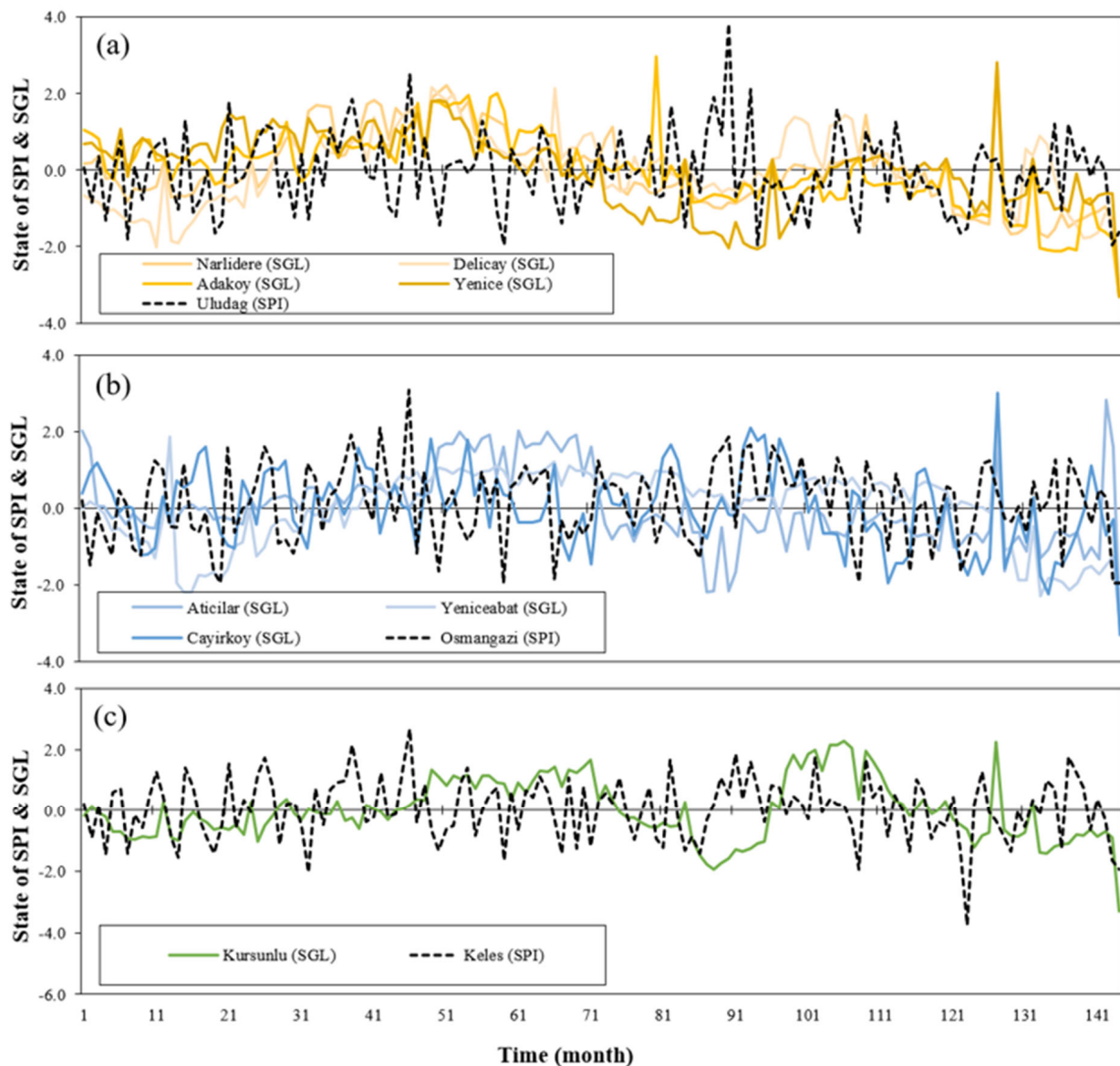
Figure 3. Time series plot of the SPI and SGL defined for the (**a**) Uludag, (**b**) Osmangazi, and (**c**) Keles regions determined by means of Thiessen polygon classification detailed in Figure 1.

In the subsequent phase, aimed at substantiating the link between groundwater and precipitation, SPI durations are prognosticated utilizing SGL durations randomly drawn from the duration curves (as depicted in Figure 5). During this process, the Thiessen polygons and SVM techniques are employed interchangeably to determine the ensemble of groundwater observation wells (Scenarios) utilized as predictors for SPI duration at the meteorological stations.

The Thiessen polygons approach suggests (Figure 1) the inclusion of the Narlidere, Delicay, Adakoy, and Yenice observation wells in estimating SPI duration at the Uludag meteorological station. Similarly, according to the Thiessen method, the Aticilar, Yenice-abat, and Cayirkoy observation wells should be incorporated to ascertain SPI durations in Osmangazi, while the Kursunlu observation well is identified as being pertinent for determining SPI duration at the Keles station.

Figure 4. Cross-correlation diagram indicating the lagged interaction of SPI in the Osmangazi, Keles, and Uludag stations with the SGL in (**a**) Narlidere, (**b**) Delicay, (**c**) Adakoy, (**d**) Aticilar, (**e**) Yeniceabat, (**f**) Cayirkoy, (**g**) Kursunlu, and (**h**) Yenice.
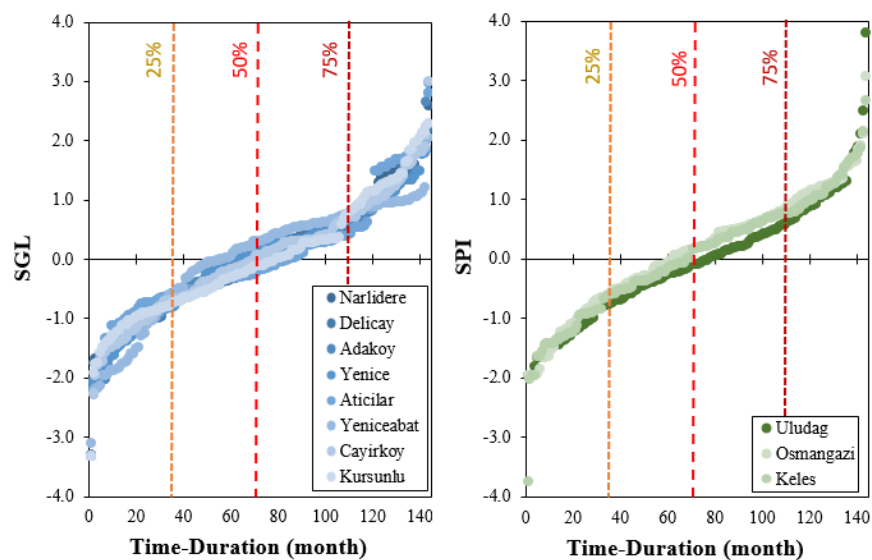
Figure 5. Drought duration curve for SGL and SPI.

Conversely, the SVM approach recommends the utilization of specific observation wells (as detailed in Table 2) for forecasting SPI durations at the Keles, Uludag, and Osmangazi stations, based on various kernel functions, including dot, radial, polynomial, neural, ANOVA, and Epachnenikov kernels. According to the results outlined in Table 2, the SPI duration at the Uludag station exhibits a significant association with most of the groundwater level records, except those from Yenice and Yeniceabat. Despite the geographic distance between Yeniceabat and the Uludag station, the findings align with those obtained via the Thiessen polygons method, which suggests the inclusion of SGL records from the Yenice observation well in estimating SPI durations in Uludag. Similarly, the SVM method posits that the Narlidere observation-well records should be included in determining the SPI in Osmangazi, while Narlidere, Yeniceabat, and Kursunlu observation-well records should be excluded from the estimation of SPI durations at the Keles station. Notably, despite Narlidere's geographical distance from the Osmangazi station, the results pertaining to the Keles station exhibit substantial disparities, notably in rejecting the role of SPI duration in the SGL duration at the Kursunlu observation well—a unique groundwater observation well introduced in the prior Thiessen-based stage.

Table 2. Selection of the best groundwater observation wells for the prediction of SPI based on the SVM method (grey highlights indicate the significant kernels larger than 0.75 that used in selection of the stations).

	Kernel	Groundwater Wells							
		Narlidere	Delicay	Adakoy	Yenice	Aticilar	Yeniceabat	Cayirkoy	Kursunlu
Uludag	Dot	0.41	0.56	0.00	0.14	0.08	0.57	1.00	0.98
	Radial	0.56	0.56	1.00	0.62	0.68	0.00	0.93	0.41
	Polynomial	0.65	1.00	0.00	0.50	0.02	0.23	0.59	0.63
	Neural	0.66	0.00	0.65	0.41	1.00	0.40	0.44	0.57
	ANOVA	0.66	0.79	0.72	0.72	0.79	0.00	1.00	0.52
	Epachnenikov	0.77	0.44	0.82	0.82	1.00	0.00	0.65	0.49
Osmangazi	Dot	0.01	0.63	0.46	0.52	0.00	1.00	0.36	0.86
	Radial	0.28	0.21	1.00	0.53	0.43	0.00	0.66	0.44
	Polynomial	0.69	1.00	0.00	0.56	0.10	0.13	0.62	0.73
	Neural	0.66	0.00	0.65	0.41	1.00	0.40	0.44	0.57
	ANOVA	0.29	0.00	1.00	0.46	0.39	0.04	0.75	0.61
	Epachnenikov	0.66	0.39	1.00	0.62	0.89	0.00	0.59	0.25
Keles	Dot	0.49	1.00	0.41	0.08	0.00	0.55	0.86	0.28
	Radial	0.36	0.48	1.00	0.51	0.70	0.00	0.76	0.44
	Polynomial	0.73	1.00	0.00	0.59	0.02	0.29	0.67	0.69
	Neural	0.66	0.00	0.65	0.41	1.00	0.40	0.44	0.57
	ANOVA	0.26	0.29	0.67	0.29	1.00	0.04	0.70	0.00
	Epachnenikov	0.19	0.24	1.00	0.36	0.16	0.00	0.61	0.01

Hence, in order to conduct further scrutiny and validate the outcomes derived from the Thiessen and SVM methodologies, we proceeded to estimate SPI durations using the corresponding SGL durations at the recommended observation wells through the ENN-FA approach. Initially, the ENN was employed to gauge SPI durations, and subsequently, the FA algorithm was deployed to bolster the performance metrics and assess the potential for scenario-models to yield superior results. In this context, Table 3 furnishes a comprehensive evaluation of the ENN-FA approach's performance in delineating the relationship between SPI and SGL during the testing phase. The resultant findings are also graphically illustrated in the box and whisker plots featured in Figure 6.

Table 3. Results obtained for the ENN-FA models based on the groundwater selection scenarios at the test stage.

	Selection	Method	NRMSE (%)	NSE	bR^2	KGE
Uludag	Thiessen	ENN-FA	13.0	0.98	0.96	0.96
	SVM	Dot-ENN-FA	13.9	0.98	0.95	0.91
		Radial-ENN-FA	12.8	0.98	0.97	0.93
		Polynomial-ENN-FA	12.8	0.98	0.93	0.83
		Neural-ENN-FA	25.3	0.93	0.83	0.88
		ANOVA-ENN-FA	14.7	0.98	0.95	0.9
		Epachnenikov-ENN-FA	14.2	0.98	0.96	0.9
Osmangazi	Thiessen	ENN-FA	12.4	0.98	0.94	0.49
	SVM	Dot-ENN-FA	13.4	0.98	0.93	0.53
		Radial-ENN-FA	30.8	0.9	0.69	−0.17
		Polynomial-ENN-FA	21.3	0.95	0.8	0.09
		Neural-ENN-FA	36.8	0.86	0.63	0.67
		ANOVA-ENN-FA	7.8	0.99	0.97	0.86
		Epachnenikov-ENN-FA	10.5	0.99	0.97	0.71
Keles	Thiessen	ENN-FA	14.2	0.98	0.94	0.8
	SVM	Dot-ENN-FA	7.4	0.99	0.97	0.95
		Radial-ENN-FA	7.8	0.99	0.97	0.97
		Polynomial-ENN-FA	7.7	0.99	0.97	0.95
		Neural-ENN-FA	24.6	0.94	0.85	0.56
		ANOVA-ENN-FA	24.6	0.94	0.85	0.56
		Epachnenikov-ENN-FA	14.2	0.98	0.92	0.91
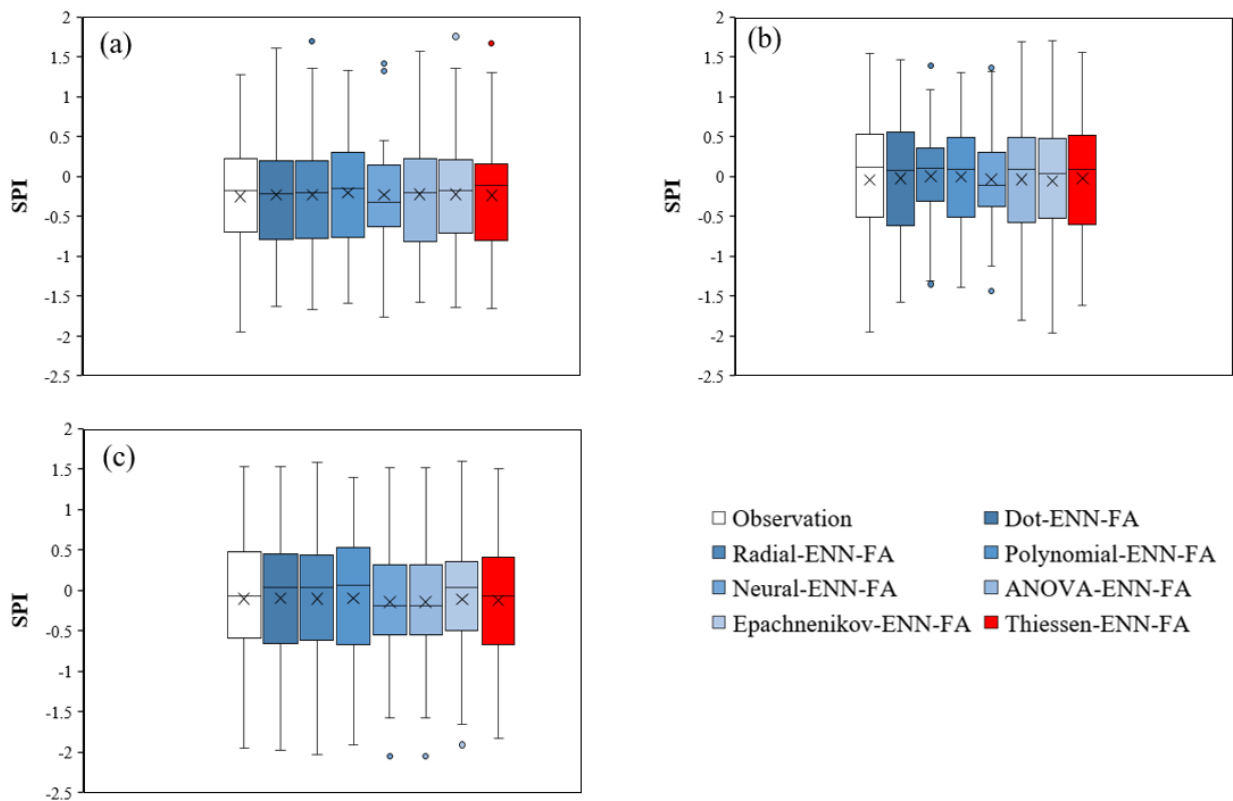
Figure 6. Box and whisker plots of the obtained results in the test stage for the (**a**) Uludag, (**b**) Osmangazi, and (**c**) Keles stations.

As delineated in Table 3, it is apparent that SVM generally yields more favorable outcomes in comparison to the Thiessen method. This essentially underscores the fact that geographic proximity and mathematical approaches may fall short in encapsulating the intricate hydrogeological dynamics. Nevertheless, in scenarios where no alternatives are available or simpler methodologies are preferred, the Thiessen polygon method retains its reliability.

When we focus on SVM as the most effective scenario-model predictor, it becomes evident that Radial-ENN-FA for Uludag, ANOVA-ENN-FA for Osmangazi, and Dot-ENN-FA for Keles can be seen as the best-performing combinations, displaying minimal bias and high efficacy. However, when addressing outliers and probability distributions (including mean, median, quartiles, etc.), Polynomial-ENN-FA for Uludag, Epachnenikov-ENN-FA for Osmangazi, and Dot-ENN-FA for Keles emerge as the superior choices. Given the close correlation among the performance metrics for the scenario-models presented in Table 3, one may find it prudent to employ a scatter plot approach to ensure compliance with both outcome probability and outlier criteria. Consequently, in cases where information is lacking or geological data are absent, this approach may serve as a robust means for achieving successful predictions.

The degree of association and predictability of SPI with the assistance of SGL also attests to the natural connection between groundwater and precipitation in the region. Consequently, it is more plausible that groundwater disturbances in the region are a consequence of climatic factors rather than anthropogenic influences. This holds particular relevance in regions like Bursa, where groundwater is not heavily relied upon as the primary water source. Nevertheless, given the increasing prevalence of drought and population growth in the area, it is foreseeable that more comprehensive investigations will be necessitated in the near future to elucidate the behavior of groundwater levels in the region.

4. Conclusions

In this research, we conducted an in-depth investigation into the nexus between meteorological drought and fluctuations in groundwater levels in the vicinity of Mount Uludag in Bursa, Turkey. Employing a rigorous analytical approach encompassing meteorological and groundwater data from multiple observation sites, our objective was to unveil the underlying intricacies that connect SPI events and SGL disturbances within the region. Our empirical findings unveil a nuanced and intricate relationship between hydro-meteorological phenomena within the study area.

Spatial and temporal analyses have indicated that although an overt direct spatial and temporal correlation between SGL and SPI time series at the monthly scale may not be readily discernible, a more extensive-scale relationship indeed exists, underscoring the significance of the interplay between precipitation patterns and groundwater abundance. We conducted a meticulous comparison of the duration curves for SGL and SPI events, introducing the concept of employing SGL duration as a predictive measure for SPI duration.

Through the application of both the Thiessen polygon and SVM techniques, we identified the optimal observation wells that demonstrate the highest predictive capacity for SPI duration at meteorological sites. Our results showcased the consistency and complementarity of insights provided by both methodologies in elucidating the connection between meteorological and groundwater occurrences. Furthermore, we harnessed the power of the ENN fine-tuned via the FA to forecast SPI durations utilizing SGL durations. This novel approach enabled us to explore the feasibility of accurately forecasting meteorological events based on groundwater behavior. Our analysis unveiled that the ENN-FA models yielded promising results, furnishing enhanced insights into the intricate relationship between SPI and SGL durations.

The present study significantly contributes to an improved comprehension of the complex dynamics governing the interplay between meteorological drought and groundwater

level fluctuations. While the detection of short-term associations may pose challenges, our findings robustly support the existence of a broader nexus between precipitation patterns and groundwater abundance. The amalgamation of innovative methodologies, encompassing SVM, ENN-FA, and duration curve analysis, represents a comprehensive approach for unraveling these intricate relationships. Future research endeavors could delve deeper into the influence of various hydrogeological factors on these observed associations, thereby facilitating the development of more robust predictive models.

Author Contributions: Conceptualization, B.V., B.M. and M.J.S.S.; methodology, B.V. and B.M.; software, B.V. and B.M.; validation, B.V. and B.M.; formal analysis, B.V.; investigation, M.J.S.S.; resources, B.V. and B.M.; data curation, B.V.; writing—original draft preparation, B.V., B.M. and M.J.S.S.; writing—review and editing, M.J.S.S.; visualization, B.V. All authors have read and agreed to the published version of the manuscript.

Institutional Review Board Statement: Not applicable.

Informed Consent Statement: Not applicable.

Data Availability Statement: The data used in this study will be available from the corresponding author upon reasonable request.

Conflicts of Interest: The authors declare no conflict of interest.

References

1. Elahi, E.; Khalid, Z.; Tauni, M.Z.; Zhang, H.; Lirong, X. Extreme Weather Events Risk to Crop-Production and the Adaptation of Innovative Management Strategies to Mitigate the Risk: A Retrospective Survey of Rural Punjab, Pakistan. *Technovation* **2022**, *117*, 102255. [CrossRef]
2. Abbas, A.; Waseem, M.; Ullah, W.; Zhao, C.; Zhu, J. Spatiotemporal Analysis of Meteorological and Hydrological Droughts and Their Propagations. *Water* **2021**, *13*, 2237. [CrossRef]
3. Sarwar, A.N.; Waseem, M.; Azam, M.; Abbas, A.; Ahmad, I.; Lee, J.E.; Haq, F.U. Shifting of Meteorological to Hydrological Drought Risk at Regional Scale. *Appl. Sci.* **2022**, *12*, 5560. [CrossRef]
4. Raziei, T.; Saghafian, B.; Paulo, A.A.; Pereira, L.S.; Bordi, I. Spatial Patterns and Temporal Variability of Drought in Western Iran. *Water Resour. Manag.* **2009**, *23*, 439–455. [CrossRef]
5. Sirdaş, S.; Şen, Z. Spatio-Temporal Drought Analysis in the Trakya Region, Turkey. *Hydrol. Sci. J.* **2003**, *48*, 809–820. [CrossRef]
6. Nalbantis, I.; Tsakiris, G. Assessment of Hydrological Drought Revisited. *Water Resour. Manag.* **2009**, *23*, 881–897. [CrossRef]
7. Yihdego, Y.; Vaheddoost, B.; Al-Weshah, R.A. Drought Indices and Indicators Revisited. *Arab. J. Geosci.* **2019**, *12*, 69. [CrossRef]
8. Groundwater Resource Management | IAEA. Available online: https://www.iaea.org/topics/groundwater (accessed on 19 September 2023).
9. Drought and Groundwater Levels | U.S. Geological Survey. Available online: https://www.usgs.gov/special-topics/water-science-school/science/drought-and-groundwater-levels (accessed on 19 September 2023).
10. Van Lanen, H.A.J.; Peters, E. Definition, Effects and Assessment of Groundwater Droughts. In *Drought and Drought Mitigation in Europe*; Springer: Dordrecht, The Netherlands, 2000; pp. 49–61. [CrossRef]
11. Kaplan, D.; Muñoz-Carpena, R.; Ritter, A. Untangling Complex Shallow Groundwater Dynamics in the Floodplain Wetlands of a Southeastern U.S. Coastal River. *Water Resour. Res.* **2010**, *46*, 8528. [CrossRef]
12. Xu, X.; Huang, G.; Qu, Z.; Pereira, L.S. Using MODFLOW and GIS to Assess Changes in Groundwater Dynamics in Response to Water Saving Measures in Irrigation Districts of the Upper Yellow River Basin. *Water Resour. Manag.* **2011**, *25*, 2035–2059. [CrossRef]
13. Elli, E.F.; Archontoulis, S.V. Dissecting the Contribution of Weather and Management on Water Table Dynamics under Present and Future Climate Scenarios in the US Corn Belt. *Agron. Sustain. Dev.* **2023**, *43*, 36. [CrossRef]
14. Bloomfield, J.P.; Marchant, B.P. Analysis of Groundwater Drought Building on the Standardised Precipitation Index Approach. *Hydrol. Earth Syst. Sci.* **2013**, *17*, 4769–4787. [CrossRef]
15. Liu, B.; Zhou, X.; Li, W.; Lu, C.; Shu, L. Spatiotemporal Characteristics of Groundwater Drought and Its Response to Meteorological Drought in Jiangsu Province, China. *Water* **2016**, *8*, 480. [CrossRef]
16. Khan, N.; Sachindra, D.A.; Shahid, S.; Ahmed, K.; Shiru, M.S.; Nawaz, N. Prediction of Droughts over Pakistan Using Machine Learning Algorithms. *Adv. Water Resour.* **2020**, *139*, 103562. [CrossRef]

17. Belayneh, A.; Adamowski, J.; Khalil, B.; Quilty, J. Coupling Machine Learning Methods with Wavelet Transforms and the Bootstrap and Boosting Ensemble Approaches for Drought Prediction. *Atmos. Res.* **2016**, *172–173*, 37–47. [CrossRef]
18. Guo, C.; Lu, J.; Tian, Z.; Guo, W.; Darvishan, A. Optimization of Critical Parameters of PEM Fuel Cell Using TLBO-DE Based on Elman Neural Network. *Energy Convers. Manag.* **2019**, *183*, 149–158. [CrossRef]
19. Ali, B.; Lashari, S.A.; Sharif, W.; Khan, A.; Ullah, K.; Ramli, D.A. An Efficient Learning Weight of Elman Neural Network with Chicken Swarm Optimization Algorithm. *Procedia Comput. Sci.* **2021**, *192*, 3060–3069. [CrossRef]
20. Kumar, D.; Gandhi, B.G.R.; Bhattacharjya, R.K. Firefly Algorithm and Its Applications in Engineering Optimization. *Model. Optim. Sci. Technol.* **2020**, *16*, 93–103. [CrossRef]
21. Mohammadi, B. Modeling Various Drought Time Scales via a Merged Artificial Neural Network with a Firefly Algorithm. *Hydrology* **2023**, *10*, 58. [CrossRef]
22. Archibald, R.; Fann, G. Feature Selection and Classification of Hyperspectral Images with Support Vector Machines. *IEEE Geosci. Remote Sens. Lett.* **2007**, *4*, 674–677. [CrossRef]
23. Maldonado, S.; Weber, R.; Basak, J. Simultaneous Feature Selection and Classification Using Kernel-Penalized Support Vector Machines. *Inf. Sci.* **2011**, *181*, 115–128. [CrossRef]
24. Imbach, T. Deep Groundwater Circulation in the Tectonically Active Area of Bursa, Northwest Anatolia, Turkey. *Geothermics* **1997**, *26*, 251–278. [CrossRef]
25. Korkmaz, S.; Türkkan, G.E. A Numerical Groundwater Flow Model of Bursa Basköy Aquifer. In Sustainable Hydraulics in the Era of Global Change, Proceedings of the 4th European Congress of the International Association of Hydroenvironment Engineering and Research, IAHR 2016, Liege, Belgium, 27–29 July 2016; Routledge: Boca Raton, FL, USA, 2016.
26. Korkmaz, S.; Keskin, M.Z. Numerical Model of Groundwater Flow Using MODFLOW: Application to Western Bursa, Turkey. In Proceedings of the 11th World Congress on Water Resources nd Environment: Managing Water Resources for a Sustainable Future-EWRA 2019, Madrid, Spain, 25–29 June 2019.
27. Kottek, M.; Grieser, J.; Beck, C.; Rudolf, B.; Rubel, F. World Map of the Köppen-Geiger Climate Classification Updated. *Meteorol. Z.* **2006**, *15*, 259–263. [CrossRef] [PubMed]
28. Mckee, T.B.; Doesken, N.J.; Kleist, J. The relationship of drought frequency and duration to time scales. In Proceedings of the 8th Conference on Applied Climatology, Anaheim, CA, USA, 17–22 January 1993; pp. 17–22.
29. Aksoy, H. Use of Gamma Distribution in Hydrological Analysis. *Turk. J. Eng. Environ. Sci.* **2000**, *24*, 419–428.
30. Vaheddoost, B.; Safari, M.J.S. Application of Signal Processing in Tracking Meteorological Drought in a Mountainous Region. *Pure Appl. Geophys.* **2021**, *178*, 1943–1957. [CrossRef]
31. Gunn, S.R. Support Vector Machines for Classification and Regression. *ISIS Tech. Rep.* **1998**, *14*, 5–16.
32. Sugumaran, V.; Muralidharan, V.; Ramachandran, K.I. Feature Selection Using Decision Tree and Classification through Proximal Support Vector Machine for Fault Diagnostics of Roller Bearing. *Mech. Syst. Signal Process.* **2007**, *21*, 930–942. [CrossRef]
33. Cervantes, J.; Garcia-Lamont, F.; Rodríguez-Mazahua, L.; Lopez, A. A Comprehensive Survey on Support Vector Machine Classification: Applications, Challenges and Trends. *Neurocomputing* **2020**, *408*, 189–215. [CrossRef]
34. Kurniawati, I.; Pardede, H.F. Hybrid Method of Information Gain and Particle Swarm Optimization for Selection of Features of SVM-Based Sentiment Analysis. In Proceedings of the 2018 International Conference on Information Technology Systems and Innovation, ICITSI 2018, Bandung, Indonesia, 22–26 October 2018; pp. 1–5. [CrossRef]
35. Danandeh Mehr, A.; Vaheddoost, B.; Mohammadi, B. ENN-SA: A Novel Neuro-Annealing Model for Multi-Station Drought Prediction. *Comput. Geosci.* **2020**, *145*, 104622. [CrossRef]
36. Zhang, X.; Zhang, Q.; Zhang, G.; Nie, Z.; Gui, Z. A Hybrid Model for Annual Runoff Time Series Forecasting Using Elman Neural Network with Ensemble Empirical Mode Decomposition. *Water* **2018**, *10*, 416. [CrossRef]
37. Li, C.; Zhu, L.; He, Z.; Gao, H.; Yang, Y.; Yao, D.; Qu, X. Runoff Prediction Method Based on Adaptive Elman Neural Network. *Water* **2019**, *11*, 1113. [CrossRef]
38. Lu, C.; Li, S.; Lu, Z. Building Energy Prediction Using Artificial Neural Networks: A Literature Survey. *Energy Build.* **2022**, *262*, 111718. [CrossRef]
39. Li, X.; Han, Z.; Zhao, T.; Zhang, J.; Xue, D. Modeling for Indoor Temperature Prediction Based on Time-Delay and Elman Neural Network in Air Conditioning System. *J. Build. Eng.* **2021**, *33*, 101854. [CrossRef]
40. Mei, G.; Zhang, H.; Zhang, B. Improving Elman Neural Network Model via Fusion of New Feedback Mechanism and Genetic Algorithm. In Proceedings of the PIC 2016, 2016 IEEE International Conference on Progress in Informatics and Computing, Shanghai, China, 23–25 December 2017; pp. 69–73. [CrossRef]
41. Toha, S.F.; Tokhi, M.O. Mlp and Elman Recurrent Neural Network Modelling for the TRMS. In Proceedings of the 2008 7th IEEE International Conference on Cybernetic Intelligent Systems, CIS 2008, Chengdu, China, 21–24 September 2008. [CrossRef]
42. Ding, S.; Zhang, Y.; Chen, J.; Jia, W. Research on Using Genetic Algorithms to Optimize Elman Neural Networks. *Neural Comput. Appl.* **2013**, *23*, 293–297. [CrossRef]
43. Yang, X.S.; He, X. Firefly Algorithm: Recent Advances and Applications. *Int. J. Swarm Intell.* **2013**, *1*, 36. [CrossRef]
44. Zambrano-Bigiarini, M. Package "hydroGOF"—Goodness-of-Fit Functions for Comparison of Simulated and Observed Hydrological Time Series. R Package. 2017. Available online: https://cran.r-project.org/src/contrib/Archive/hydroGOF/ (accessed on 19 September 2023).

45. Han, Z.; Huang, S.; Huang, Q.; Leng, G.; Wang, H.; Bai, Q.; Zhao, J.; Ma, L.; Wang, L.; Du, M. Propagation Dynamics from Meteorological to Groundwater Drought and Their Possible Influence Factors. *J. Hydrol.* **2019**, *578*, 124102. [CrossRef]
46. Gong, R.; Chen, J.; Liang, Z.; Wu, C.; Tian, D.; Wu, J.; Li, S.; Zeng, G. Characterization and Propagation from Meteorological to Groundwater Drought in Different Aquifers with Multiple Timescales. *J. Hydrol. Reg. Stud.* **2023**, *45*, 101317. [CrossRef]